Chinese Journal of Catalysis 48 (2023) 235–246

available at www.sciencedirect.com

ScienceDirect

journal homepage: www.sciencedirect.com/journal/chinese-journal-of-catalysis

Article

Activation of partial metal sites in high-entropy oxides for enhancing thermal and electrochemical catalysis

Jinxing Mi [a,1], Xiaoping Chen [b,1], Yajun Ding [a], Liangzhu Zhang [a], Jun Ma [c], Hui Kang [c], Xianhong Wu [a], Yuefeng Liu [c], Jianjun Chen [b,*] , Zhong-Shuai Wu [a,*]

[a] *State Key Laboratory of Catalysis, Dalian Institute of Chemical Physics, Chinese Academy of Sciences, Dalian 116023, Liaoning, China*
[b] *State Key Joint Laboratory of Environment Simulation and Pollution Control, School of Environment, Tsinghua University, Beijing 100084, China*
[c] *Dalian National Laboratory for Clean Energy, Dalian Institute of Chemical Physics, Chinese Academy of Sciences, Dalian 116023, Liaoning, China*

ARTICLE INFO

Article history:
Received 3 January 2023
Accepted 8 February 2023
Available online 20 April 2023

Keywords:
High entropy oxides
Solid phase combustion
Metal sites activation
Catalytic redox
Li-O_2 battery

ABSTRACT

High-entropy oxides (HEOs) have been tentatively and prospectively applied for chemical catalysis and energy storage. However, further enhancing their performance is difficult owing to the difficulty in precisely regulating the physical-chemical properties. In this work, a general in-situ modulation strategy of solid-phase combustion involving thiourea addition and alkali liquor treatment is developed to activate metal sites and lattice oxygen species of CuCoNiZnAl HEOs. Consequently, compared with pristine HEOs, the activated HEOs not only display higher CO_2 hydrogenation and CO oxidation activities but also significantly enhanced electrocatalytic performance (discharge/charge capacities of 12049/9901 mAh/g) with excellent cycle stability (2500 h) for Li-O_2 batteries. The superior performance of the activated HEOs is attributed to its facile electron transferability. This simple and effective strategy could be easily applied on a large scale, guiding the development of highly active heterogeneous HEO catalysts for various functional applications.

1. Introduction

High-entropy materials have attracted extensive interest from researchers in many fields by virtue of the tunability of their constituent elements into one specific lattice structure, superior mechanical/heat stability under harsh conditions, and simplicity of the preparation process [1–3]. In particular, high-entropy oxides (HEOs), an emerging category of metal oxides, have limited yet impressive applications in catalysis and energy storage [4]. Both single-phase HEOs and mixed-phase HEOs are collectively regarded as HEOs and have been rapidly developed [5]. Constituted by at least five metal cations into one pure or mixed lattice phase, the formation of HEOs is driven by entropy, endowing them with superior thermodynamic stability, exclusive synergistic effects, multifarious phase structures, and tunable electronic structures [5]. As a result, the various preparation methods and potential functional applications of HEOs have stimulated research interest. Meanwhile, the structure and characteristics of HEOs have also been studied in depth, as the five or more metallic elements comprising HEOs are usually present in equimolar ratios and distributed randomly in the HEO framework. This leads to unexpectedly

---

* Corresponding author. E-mail: chenjianjun@tsinghua.edu.cn (J. Chen), wuzs@dicp.ac.cn (Z.-S. Wu).
[1] Contributed equally to this work.

This work was supported by the China Postdoctoral Science Foundation (2021M693125), Dalian Innovation Support Plan for High Level Talents (2019RT09), Dalian National Laboratory for Clean Energy (DNL), CAS, DNL Cooperation Fund, CAS (DNL202016, DNL202019), The Joint Fund of the Yulin University, and the Dalian National Laboratory for Clean Energy (YLU-DNL Fund 2021002, YLU-DNL Fund 2021009).
https://doi.org/10.1016/S1872-2067(23)64409-2

strong metal-support interactions, excellent redox properties, stable chemical states, and abundant physical-chemical properties [6]. As a result, the variable metallic element composition and crystal structure of HEOs could be amenable to various applications such as thermocatalysis, electrocatalysis [7,8], and lithium-ion storage [9]. Taking catalysis as an example, HEOs could be directly used as pure catalysts [10]. Furthermore, when combined with different functional materials (e.g., metal-organic frameworks, composite oxides) or noble metals (e.g., Pt, Pd), the generated composited HEOs could realize excellent catalytic performance for multifarious functional applications [4,11,12].

As mentioned above, the unique structure and abundant physical-chemical properties have enabled their successful catalytic application in certain redox reactions (e.g., CO oxidation, CO_2 hydrogenation). For example, Zhang *et al.* [13] developed highly mesoporous, Cu-based HEOs using a sol-gel method. The HEOs exhibited impressive CO oxidation performance at high temperature (> 200 °C). To further improve the low-temperature catalytic activity of HEOs toward CO oxidation, Chen *et al.* [14] reported an HEO-based catalyst prepared by combining HEOs with $CuCeO_x$. As a result, CO could be catalytically converted over the composited $MCuCeO_x$-HEOs at much lower temperatures (< 50 °C). Meanwhile, higher reaction temperatures could still enhance CO conversion with excellent stability. Moreover, the combination of noble metals with HEOs could maximally optimize CO catalytic oxidation conversion. For example, Chen *et al.* [15] designed a mechanochemistry route to prepare Pt-based HEOs ($PtNiMgCuZnCoO_x$ HEOs), and the addition of Pt species (only 0.3 wt% Pt) over HEOs could effectively accelerate the conversion of CO (particularly at low temperature) when compared with $NiMgCuZnCoO_x$ HEOs, which was induced by the generation of Pt-O-M species over $PtNiMgCuZnCoO_x$ HEOs. Unexpectedly, the stable structure of HEOs also endowed the $PtNiMgCuZnCoO_x$ HEOs with superior thermostability. Apart from Pt, multifarious noble species (e.g., Ru, Au, Pd) have also been combined with HEOs to further improve CO conversion under complicated conditions [16–18]. Apart from catalytic oxidation, HEOs are also promising for catalytic reduction reactions. For instance, Zhang *et al.* [19] designed cubic HEOs $Zr_{0.5}(NiFeCuMnCo)_{0.5}O_x$ using a solvent-free approach to convert CO_2 via catalytic hydrogenation. They found that $Zr_{0.5}(NiFeCuMnCo)_{0.5}O_x$ not only displayed better CO_2 conversion performance than that of doped $Zr_{0.5}M_{0.5}O_x$ (M = Cu, Fe, CuMn, etc.) catalysts at 400 °C but also exhibited excellent stability (i.e., as long as 500 h – much longer than that of $Zr_{0.5}(MnCu)_{0.5}O_x$). Similarly, when combined with noble metals, the obtained functionalized HEOs also demonstrated enhanced CO_2 hydrogenation performance. As reported by Chen *et al.* [20] found that by introducing a noble metal (Ru or Pt) into (NiMgCuZnCo)O, the as-obtained Ru/Pt-based (NiMgCuZnCo)O catalysts displayed impressive CO_2 conversion (> 40%) at high temperature (500 °C) with high CO selectivity (> 95%) in a stable state. This conversion was much higher than that of pure (NiMgCuZnCo)O. These studies highlighted the significance of HEOs and their derived catalysts in catalytic applications, suggesting the importance of developing HEOs for further applications. However, the reported optimized strategies (such as the introduction of noble metals) are not the most simple and effective solutions for further improving the properties and performance of HEOs and thus are not amenable to their commercial preparation and industrial application.

In this work, we propose an *in-situ* strategy to activate partial metal sites and induce lattice oxygen (O_{latt}) species in CuCoNiZnAl HEOs (referred to as CuCoNiZnAl hereafter) by adding thiourea using a solvent-free method to produce CuCoNiZnAl-T (where T stands for thiourea). The CuCoNiZnAl-T activated species were further exposed through alkali liquor treatment to obtain CuCoNiZnAl-T-NaOH. Subsequently, the physical-chemical properties of these HEOs were analyzed using various characterization techniques. Meanwhile, CO_2 hydrogenation, CO oxidation, and the lithium oxygen (Li-O_2) battery were chosen to evaluate and compare the performance of the obtained HEOs. Thiourea addition during the calcination process was verified to change the HEO microenvironment, activating the partial metal sites along with the surface O_{latt} species and promoting the reduction properties of the HEOs, which were further optimized by the alkali liquor treatment. It was revealed that the electrons could be easily transferred between the activated Cu, Co, and Ni oxides and surface O_{latt} species, leading to the enhanced redox properties of the HEOs and improved catalytic/energy storage performance. Finally, the relationship between the ameliorative properties and enhanced application performance is discussed and established. To the best of our knowledge, this is the first study reporting the activation regulation of HEOs by the simple inclusion of thiourea using a solvent-free method and alkali liquor treatment for application in the fields of thermal and electrochemical catalysis.

2. Experimental

2.1. Catalyst preparation

All Cu-based HEOs catalysts were obtained using mechanochemistry methods. For example, CuCoNiZnAl HEOs (abbreviated as CuCoNiZnAl), equimolar (0.02 mol) $Cu(NO_3)_2\cdot6H_2O$, $Co(NO_3)_2\cdot6H_2O$, $Ni(NO_3)_2\cdot6H_2O$, $Zn(NO_3)_2\cdot6H_2O$, and $Al(NO_3)_3\cdot9H_2O$ were weighed and physically mixed in an agate mortar until a blue powder was formed. Afterwards, the mixed powders were calcinated in air at 900 °C for 4 h at a heating rate of 3 °C/min to obtain the desired crystalline oxide phase. CuCoNiZnAl enhanced with thiourea (CuCoNiZnAl-T) was prepared using the same method as that used to prepare CuCoNiZnAl, but 0.05 mol thiourea was added during the mixture of the metal complexes. As for the modified CuCoNiZnAl-T in NaOH solution (labeled CuCoNiZnAl-T-NaOH), the obtained CuCoNiZnAl-T (1.2 g) was added to NaOH solution (5 mol/L, 30 mL), which was further fixed in a hydrothermal reactor and treated at 110 °C for 24 h (Fig. S1). It should be noted that the alkali liquor treatment only slightly reduced the mass of CuCoNiZnAl-T, that is, no new species were formed, and the metallic elements dissolved to form CuCoNiZnAl-T-NaOH. Finally, CuCoNiZnAl-T-NaOH was centrifuged and dried. The procedure is described in more detail in the Supporting Information.

2.2. Characterizations and performance test

The physical-chemical properties, morphologies, and crystal structures of the Cu-based HEOs catalysts were elucidated using various techniques, such as X-ray diffraction (XRD), N_2 adsorption-desorption isotherms, Raman spectroscopy, electron paramagnetic resonance spectroscopy (EPR), chemisorption tests, scanning electron microscopy (SEM), high-resolution transmission electron microscopy (HRTEM), X-ray photoelectron spectroscopy (XPS). A detailed description of these characterizations can be found in the Supporting Information. The Cu-based HEOs catalysts were evaluated with respect to their performance in CO_2 hydrogenation, CO oxidation, and an Li-O_2 battery test. Detailed descriptions of the pre-treatment and performance evaluations can also be found in the Supporting Information.

3. Results and discussion

3.1. Structural properties and morphological characteristics

The XRD patterns of CuCoNiZnAl, CuCoNiZnAl-T, and CuCoNiZnAl-T-NaOH are presented in Fig. 1(a). The diffraction peaks at 31.5°, 37.1°, 45.2°, 55.7°, 59.4°, and 65.3° are assigned to the phase of spinel oxides, while those at 35.6°, 38.8°, 43.1°, and 62.5° are ascribed to the phase of compound oxides [21,22]. It is evident from the patterns that the obtained HEOs possess a mixed phase. The very similar XRD patterns of CuCoNiZnAl-T and CuCoNiZnAl-T-NaOH indicate that there is no new phase generation over the CuCoNiZnAl-T-NaOH after alkali liquor treatment. Particularly for CuCoNiZnAl-T-NaOH, no patterns of characteristic of a hydroxide-like phase are apparent. In addition, the peak intensities of the XRD spectra for CuCoNiZnAl-T and CuCoNiZnAl-T-NaOH are slightly weaker than those of CuCoNiZnAl, suggesting that the addition of thiourea along with alkali liquor treatment slightly impaired the crystallinity but did not affect the crystal structure. Aside from the phase structures, the textural parameters were also analyzed by acquiring the low-temperature N_2 adsorption-desorption isotherms. CuCoNiZnAl exhibits a type IV isotherm accompanied with very little N_2 adsorption in the relative pressure (p/p_0) range of 0–0.9 and manifests very limited mesoporosity, which is also reflected in the pore-size distribution (inset of Fig. 1(b)) [23]. In addition, CuCoNiZnAl-T shows a slightly higher N_2-adsorbing capacity and a more abundant pore-size distribution than that of CuCoNiZnAl, which was facilitated by the volatilization of thiourea (as a pore-enlarging agent) during the calcination process. However, although the post-alkali treatment still keeps its pore structure, the change of massive morphology to sheet morphology could bring about the partial decrease of the inner pore, which will be discussed in a later section. As a result, the total BET surface area (S_{BET}) of these HEOs gives an order of CuCoNiZnAl-T (4.8 m^2/g) > CuCoNiZnAl-T-NaOH (3.2 m^2/g) > CuCoNiZnAl (1.8 m^2/g). It should be noted that the increased textural parameters of CuCoNiZnAl-T and CuCoNiZnAl-T-NaOH are benefical to the exposure of surface metal sites and oxygen species, thereby

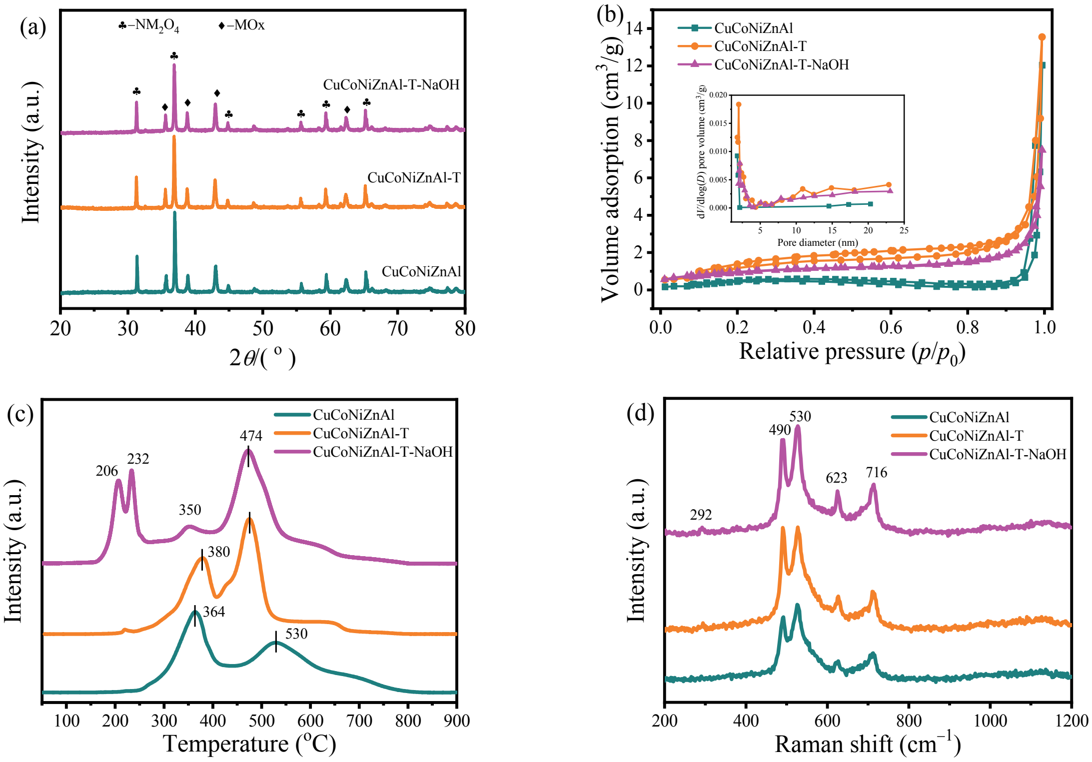

Fig. 1. XRD patterns (a), N_2 adsorption-desorption isotherms (inset: pore size distribution profiles) (b), H_2-TPR profiles (c), and Raman spectra (d) of CuCoNiZnAl, CuCoNiZnAl-T, and CuCoNiZnAl-T-NaOH.

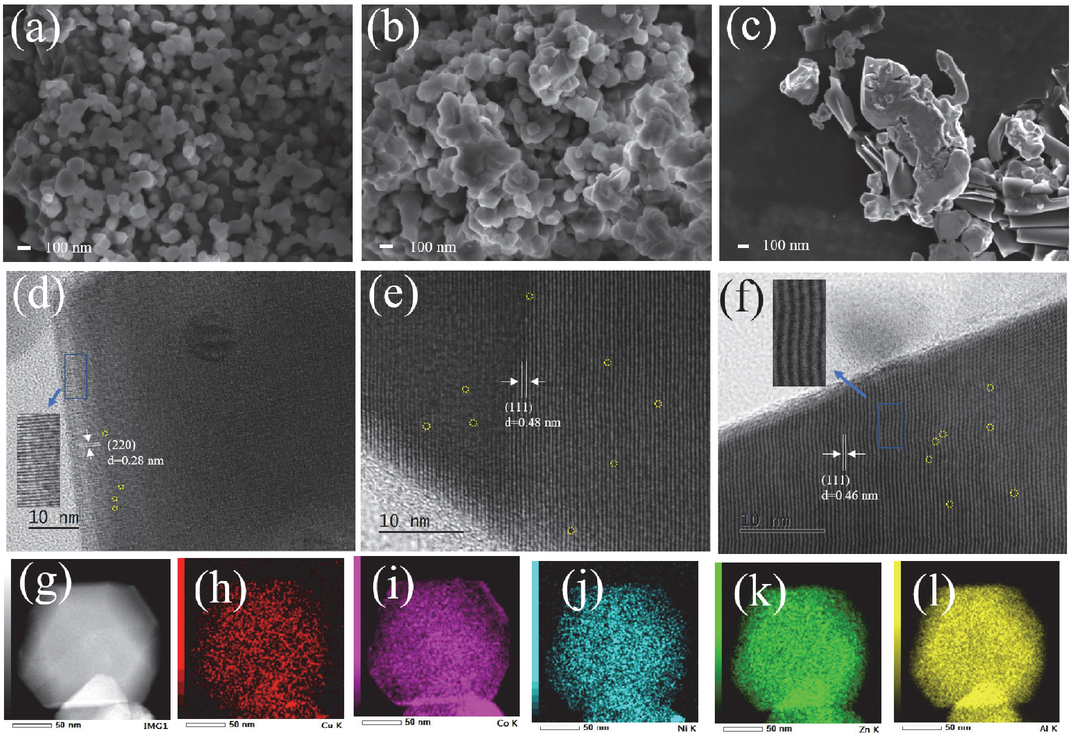

Fig. 2. SEM images of CuCoNiZnAl (a), CuCoNiZnAl-T (b), and CuCoNiZnAl-T-NaOH (c). HRTEM images of CuCoNiZnAl (d), CuCoNiZnAl-T (e), and CuCoNiZnAl-T-NaOH (f). STEM image (g) and Cu (h), Co (i), Ni (j), Zn (k), and Al (l) elemental distributions in CuCoNiZnAl-T-NaOH examined at nanometer scale using STEM-EDS.

affording sufficient space for molecular collisions, initiating a gas-phase catalytic reaction.

Subsequently, an H_2 temperature-programmed reduction (H_2-TPR) experiment was conducted to evaluate the effect of introduced thiourea and post alkaline liquor treatment on the reducibility of these HEO catalysts (Fig. 1(c)). The CuCoNiZnAl catalyst gave rise to two distinct reduction peaks at ≈ 364 and 530 °C, ascribed to the reduction of Co oxides and Ni oxides, respectively [24,25]. It is noteworthy that no reduction peaks corresponding to Cu oxides were observed in profile of the CuCoNiZnAl catalyst, possibly owing to the inhibition of the reduction of Cu oxides. In the H_2-TPR profile of the CuCoNiZnAl-T catalyst, two obvious reduction peaks at ≈ 380 and 474 °C were also observed. Compared with the profile of the CuCoNiZnAl catalyst, the position of the Co oxide reduction peak for the CuCoNiZnAl-T catalyst shifts upwards by 16 °C, and the position of the Ni oxide reduction peak shifts downwards by 56 °C, clearly indicating that the Ni oxides are activated upon introducing thiourea. Moreover, a tiny reduction peak at ≈ 220 °C emerged, which is assigned to the evolution of Cu^{2+} to Cu oxides [26,27]. It was confirmed that the introduction of thiourea also slightly activates the Cu oxides over the CuCoNiZnAl-T catalyst. As for the CuCoNiZnAl-T-NaOH catalyst, except for the optimized reduction peaks of Co/Ni oxides (reduction peak of Co oxides at 350 °C and reduction peak of Ni oxides at 474 °C), two sharp and strong reduction peaks appear at 200–250 °C. The new reduction peaks are associated with the reduction of Cu oxides (i.e., Cu^{2+} to Cu^+ at 206 °C, and Cu^+ to Cu^0 at 232 °C) [26]. Meanwhile, the Co oxide reduction peak shifts from 380 °C for CuCoNiZnAl-T to 350 °C for CuCoNiZnAl-T-NaOH with a decrease in peak area. This is possibly because the generation of the irregular flake morphology promotes the exposure of Cu species and partially inhibits the exposure of Co species. As a whole, the reducibility of the CuCoNiZnAl-T-NaOH catalyst is much better than those of CuCoNiZnAl-T and CuCoNiZnAl. Meanwhile, it is clear that the total reduction peak area of the CuCoNiZnAl-T-NaOH catalyst is larger than that of the other HEOs, which indicates the formation of a greater amount of more easily reduced Cu, Co, and Ni oxides.

Moreover, Raman spectroscopy was performed to analyze the chemical character of the Cu, Co, and Ni oxides of the HEOs (Fig. 1(d)). Four distinct peaks centered at 490, 530, 623, and 716 cm^{-1} were observed in the spectrum of CuCoNiZnAl, which are ascribed to the typical Raman-active modes of Cu oxides, Co oxides and Ni oxides [28,29]. Among them, the bands at 530 and 623 cm^{-1} are associated with the single-phonon scattering of Ni oxides and B_g vibrational modes of Cu oxides, respectively [28]. Meanwhile, the two peaks centered at 490 and 716 cm^{-1} were assigned to the E_g and A_{1g} symmetries of Co oxides, respectively [29]. Interestingly, these peaks intensified, and new peaks emerged in the spectrum of CuCoNiZnAl-T. In detail, the peaks centered at 490, 530, 623, and 716 cm^{-1} are stronger than those of CuCoNiZnAl, particularly the 490 cm^{-1} peak, which indicates the optimization of the Co oxides. In addition, one weak peak at ≈ 292 cm^{-1}, assigned to the A_g vibrational modes of the Cu oxides, is apparent [30]. The introduction of thiourea during the preparation process is believed to improve the reducibility and structural properties of the Cu, Co, and Ni oxides, which agrees well with the H_2-TPR results. After alkaline liquor treatment of CuCoNiZnAl-T, all these peaks further intensify. In summary, the mechanochemical process in this work confirmed the successful synthesis of CuCoNiZnAl, and then the *in-situ* introduction of thiourea and post-alkali liquor treatment improve the textural parameters and physical-chemical properties of both CuCoNiZnAl-T and CuCoNiZnAl-T-NaOH.

The morphology and structure of CuCoNiZnAl, CuCoNiZnAl-T, and CuCoNiZnAl-T-NaOH were further characterized. The SEM image of CuCoNiZnAl shows a relatively uniform polyhedron with a major particle size of 70–200 nm (Fig. 2(a)). After introducing thiourea during the synthesis process, the as-obtained CuCoNiZnAl-T gradually displays a deposit with an adherent polyhedron morphology (Fig. 2(b)). Some standalone polyhedra with a major particle size of 70–200 nm and interwoven heterogeneous blocks co-existed in CuCoNiZnAl-T. Further modifying CuCoNiZnAl-T with alkaline liquor, it is estimated that most of the adherent polyhedra disappear, and large, irregular flakes emerge in CuCoNiZnAl-T-NaOH. This is because the introduction of thiourea along with alkaline liquor thermal treatment destroyed the uniform polyhedral morphology and reunited the adherent polyhedra into a sheet structure (Fig. 2(c)). Meanwhile, the presence of nanosheets in CuCoNiZnAl-T-NaOH was also proven using atomic force microscopy (AFM) (Fig. S2). In short, the CuCoNiZnAl-T-NaOH obtained here possesses a folded and thin nanosheet structure. Combined with the S_{BET} result (Fig. 1(b)), it can be concluded that some inner pores are destroyed owing to the sheet structure generated in CuCoNiZnAl-T-NaOH, accounting for its slightly smaller BET surface area compared with that of CuCoNiZnAl-T.

The morphological character of these HEOs was also analyzed using TEM. As depicted in Fig. S3, CuCoNiZnAl and CuCoNiZnAl-T have an irregular, massive morphology, whereas CuCoNiZnAl-T-NaOH possesses a sheet-like morphology. Afterwards, HRTEM confirmed the different lattice states in these HEOs. As revealed in Fig. 2(d), CuCoNiZnAl shows an interplanar spacing of ≈ 0.28 nm, assigned to the *d*(220) spacing of the spinel phase. Meanwhile, CuCoNiZnAl-T and CuCoNiZnAl-T-NaOH have interplanar spacings of ≈ 0.49 and ≈ 0.45 nm, respectively, corresponding to the *d*(111) spacing of the spinel phase (Figs. 2(e) and (f)) [21]. The different lattice fringe of CuCoNiZnAl compared with those of CuCoNiZnAl-T and CuCoNiZnAl-T-NaOH confirms that the addition of thiourea along with alkali liquor treatment significantly changes the exposure of the lattice plane. Moreover, the alkali liquor treatment of CuCoNiZnAl-T could bring about the distorted lattice fringe of CuCoNiZnAl-T-NaOH (insert of Fig. 2(f)). The distorted lattice fringe of CuCoNiZnAl-T-NaOH suggests the existence of abundant surface vacancies, as confirmed by the intensity profile derived from the lattice fringe in the HRTEM images (Figs. S4–S6). In detail, dark dots (partly labeled by red circles) are evident in the line profiles of these HEOs, which are induced by the generated cationic vacancies. It is noted that the peaks indicate the intensities of the cationic sites (Cu, Co, Ni, Zn, or Al), while the valley represents the signals between lattice fringes. Among these HEOs, CuCoNiZnAl shows clear, uniform positive peaks (Fig. S4). By contrast, some uneven peaks were randomly distributed in the profiles of CuCoNiZnAl-T (Fig. S5) and CuCoNiZnAl-T-NaOH (Fig. S6), particularly in the case of the latter. Therefore, a certain amount of cationic vacancies exist in CuCoNiZnAl-T-NaOH. However, the type of cationic vacancies could not be determined owing to the complicated structural characteristics of the HEOs. Although the morphology, phase structure, and cationic vacancies are mainly affected by the addition of thiourea along with alkaline liquor thermal treatment (Figs. S5–S7) [31], the different elements in these HEOs are still uniformly distributed. Figs. 2(j)–(l) and Figs. S8–S13 exhibit the elemental distribution mappings on different scales. It can be seen that the metallic elements of CuCoNiZnAl and CuCoNiZnAl-T are well-distributed on both micrometer and nanometer scales (Figs. S8–S11). A similar phenomenon exists for CuCoNiZnAl-T-NaOH (Figs. 2(j)–(l) and Figs. S12 and S13), suggesting the successful mixture and stable distribution of metals and oxygen, even after introducing thiourea and carrying out alkaline liquor treatment. The STEM-EDS analysis further proves the successful synthesis of the mixed-phase HEOs, and the uniform distribution of elements in these HEOs is good for the strong interaction among these different metal species. Compared with the Cu and Ni species, the Co species appear to segregate more at the surface. In particular, the generated cationic vacancies and distorted lattice of CuCoNiZnAl-T-NaOH may endow it with more unique physical-chemical properties for various functional applications.

3.2. XPS and He-TPD characterizations

Apart from the surface morphological structure, XPS was used to evaluate the chemical states of the as-synthesized CuCoNiZnAl HEOs (Fig. S14 and Fig. 3(a)). Fig. S14(a) shows the survey XPS spectra of these HEO catalysts, which reveals the presence of Cu, Co, Ni, Zn, Al and O. Obviously, the surface O content of the CuCoNiZnAl-T-NaOH catalyst (47.73 at%) is much higher than those of CuCoNiZnAl-T (41.93 at%) and CuCoNiZnAl (38.47 at%), indicating that the addition of thiourea and post alkali liquor treatment exposes the surface oxygen species. In addition, the intensities of the Cu 2*p*, Co 2*p*, Ni 2*p*, Zn 2*p*, and Al 2*p* XPS peaks of CuCoNiZnAl-T-NaOH are much stronger than those of CuCoNiZnAl-T and CuCoNiZnAl (Figs. S14(b)–(f)), further confirming that the construction of the sheet structure is highly beneficial to the improvement of the surface chemical states of metallic elements and O_{latt} species. Besides the enhancement of the physical-chemical properties and morphological structure, the surface oxygen properties of CuCoNiZnAl-T-NaOH are also affected. As shown in Fig. 3(a), these HEOs give rise to two obvious O 1*s* peaks at approximately 531.3 and 529.7 eV, ascribed to the adsorbed oxygen (O_{ads}) and O_{latt} close to the surface, respectively [32,33]. In particular, the O 1*s* peak intensity at 531.1 eV is clearly weaker than that of the signal at 529.7 eV, indicating that these HEOs contain more O_{latt} species. Meanwhile, it was observed that the binding energy of the O_{latt} peaks of CuCoNiZnAl-T-NaOH and

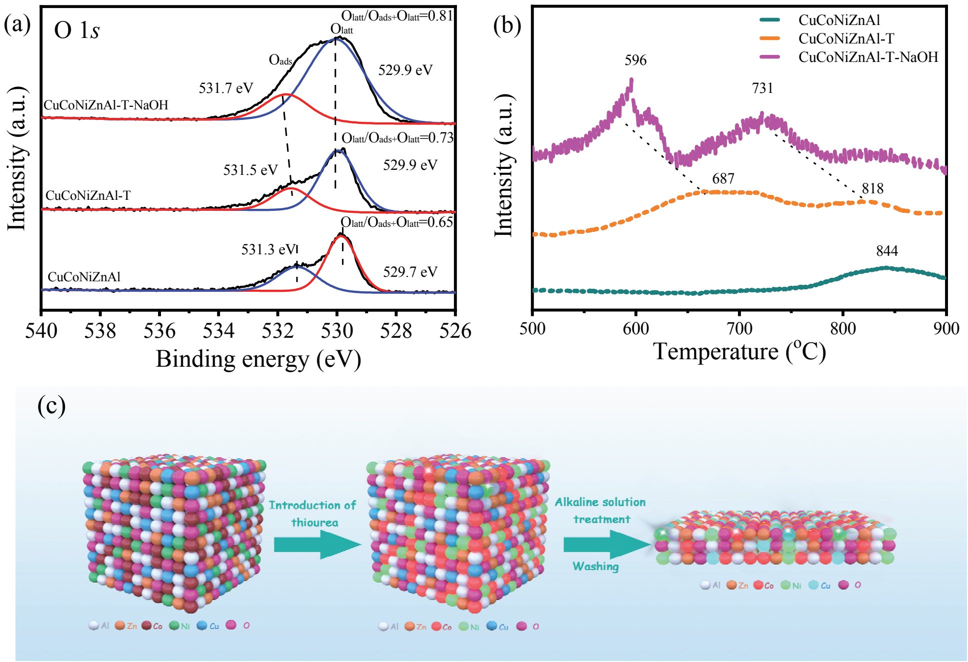

Fig. 3. O 1*s* XPS spectra (a) and He-TPD profiles (b) of CuCoNiZnAl, CuCoNiZnAl-T, and CuCoNiZnAl-T-NaOH. (c) Schematic diagram illustrating the physical-chemical property evolution from CuCoNiZnAl to CuCoNiZnAl-T and then to CuCoNiZnAl-T-NaOH.

CuCoNiZnAl-T (529.9 eV) was higher than that of CuCoNiZnAl (529.7 eV), suggesting that the O_{latt} of CuCoNiZnAl-T-NaOH and CuCoNiZnAl-T close to the surface has a higher electron-cloud density. This implies that the O_{latt} species over the CuCoNiZnAl-T-NaOH and CuCoNiZnAl-T catalysts are notably activated and thus easily participate in the catalytic redox reactions. Moreover, the O_{latt} species content of CuCoNiZnAl-T-NaOH (81%) is much higher than those of CuCoNiZnAl-T (73%) and CuCoNiZnAl (65%). According to the XPS result, CuCoNiZnAl-T-NaOH offers the highest O_{latt} species in these HEOs owing to the activated Cu, Co, and Ni oxides and sheet-like structure.

To further evaluate the effect of the introduced thiourea and sheet-structure construction on the O_{latt} species, He temperature-programmed desorption (He-TPD) was performed to evaluate the surface and bulk oxygen species of these HEOs. Usually, the desorption peak at high temperature (T > 500 °C) is derived from the released bulk O_{latt} species [34,35]. The lower desorption temperature of O_{latt} species means that the O_{latt} species is more active. As shown in Fig. 3(b), it is evident that the CuCoNiZnAl catalyst only exhibits one wide desorption peak between 700 and 900 °C, which is assigned to bulk O_{latt} species. For CuCoNiZnAl-T, one broad and asymmetric obvious desorption peak at 687 °C and one weak desorption peak at 818 °C appeared, indicating that some surface O_{latt} species and more activated bulk O_{latt} species were generated over CuCoNiZnAl-T. Meanwhile, the decomposition temperature of bulk O_{latt} oxygen species of CuCoNiZnAl-T-NaOH shifted to lower temperature, including one obvious broad and asymmetric desorption peak at 596 °C and one weak desorption peak at 731 °C. In particular, based on the He-TPD peak area, CuCoNiZnAl-T-NaOH possesses much more activated O_{latt} species compared with CuCoNiZnAl-T and CuCoNiZnAl, i.e., CuCoNiZnAl-T-NaOH > CuCoNiZnAl-T > CuCoNiZnAl. Considering this, it is demonstrated that the introduction of thiourea partly affects the chemical state of the metal site in the HEOs and further releases the O_{latt} species. However, the O_{latt} species are not obviously increased owing to the limitation of the massive morphology. Combined with the H_2-TPR result, it is speculated that the easily reduced transition metal oxides activated the bulk O_{latt} species, thereby reducing its decomposition temperature. According to the change in physical-chemical properties and morphology of these HEOs, the evolution process of the CuCoNiZnAl HEOs after thiourea addition and alkali liquor treatment was elucidated (Fig. 3(c)). Firstly, the metal species in CuCoNiZnAl were distributed randomly, which is confirmed by the XRD and EDS mapping results (Fig. 1(a) and Figs. S8–S13). When introducing thiourea into the preparation process of CuCoNiZnAl-T, its release and decomposition could affect the microenvironment during the calcination process, thereby changing the reducibility (but not the valence states) of the Co and Ni species (Fig. 1(c) and Fig. S14) and activating the Co and Ni species. Meanwhile, the alkali liquor treatment of CuCoNiZnAl-T adjusted the morphology and further activated the Cu species of CuCoNiZnAl-T-NaOH (Figs. 1(c) and (d) and Fig. 3(c)). In summary, for CuCoNiZnAl-T-NaOH, thiourea addition along with alkaline liquor treatment led to remarkably active Cu, Co, and Ni sites along with O_{latt} species; the enhanced physical-chemical properties strengthened the electron transferability, thereby potentially improving the redox reaction performance.

3.3. Catalytic performance

To evaluate the promotional effect of activated metal oxides and the sheet morphology construction on the catalytic performance of CuCoNiZnAl and modified CuCoNiZnAl catalysts for redox reactions, we first used classical CO_2 hydrogenation as a model reaction. Clearly, the reaction data (Fig. S15) reveals that all the HEOs exhibit increased CO_2 conversion from 200 to 600 °C, indicating high CO selectivity and almost no CO_2 conversion at low temperature (< 300 °C). The incomplete conversion of CO_2 to CO is caused by some methanation owing to the existence of Co and Ni species in the CuCoNiZnAl and modified CuCoNiZnAl catalysts under a CO_2 + H_2 atmosphere. By contrast, CuCoNiZnAl-T and CuCoNiZnAl-T-NaOH achieve much higher CO_2 conversion than CuCoNiZnAl in the temperature range of 350–600 °C. The calculated CO_2 conversion rate over CuCoNiZnAl is only 0.00655 and 0.02679 mmol/(g·s) at 400 and 600 °C, respectively, while over CuCoNiZnAl-T, the conversation rates at these temperatures are 0.01792 and 0.03571 mmol/(g·s), respectively (Fig. 4(a)). Excitingly, CuCoNiZnAl-T-NaOH displays a CO_2 conversion rate of 0.01837 and 0.03892 mmol/(g·s) at 400 and 600 °C, respectively. In particular, the CO_2 conversion of CuCoNiZnAl-T-NaOH is close to equilibrium conversion at high temperature (≥ 500 °C), a superior catalytic performance for CO_2 hydrogenation (Fig. S15(a)). Furthermore, the apparent activation energy (E_a) of CO_2 hydrogenation over these catalysts (Fig. S16) was calculated and found to decrease in the following order: CuCoNiZnAl (99.4 kJ/mol) > CuCoNiZnAl-T (87.2 kJ/mol) > CuCoNiZnAl-T-NaOH (74.6 kJ/mol). It is noteworthy that these HEOs also have good stability for CO_2 hydrogenation. In detail, the CuCoNiZnAl-T undergoes almost no decline in CO_2 conversion with stable, high CO selectivity (≈ 70%) in a span of 40 h at 280 °C and 2 MPa (Fig. S17); therefore, this catalyst is potentially suitable for application in complicated conditions. Among these HEO catalysts, CuCoNiZnAl-T-NaOH displays the highest

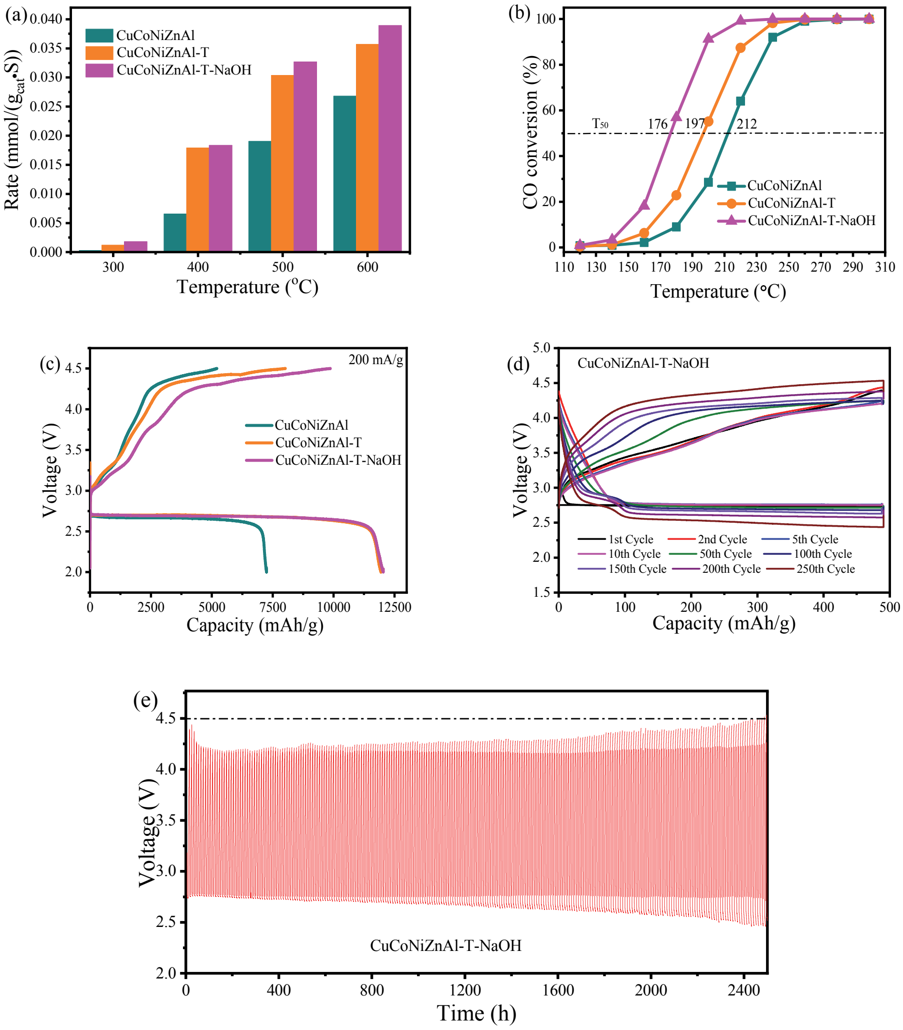

Fig. 4. (a) Rates for CO_2 hydrogenation. (b) CO conversion for CO oxidation. (c) Initial discharge-charge profiles at a current density of 200 mA/g for an Li-O_2 battery using CuCoNiZnAl, CuCoNiZnAl-T, and CuCoNiZnAl-T-NaOH as cathodes. (d) Typical discharge-charge profiles of the CuCoNiZnAl-T-NaOH cathode under a voltage range of 2.0–4.5 V at 200 mA/g. (e) Cycling performance of CuCoNiZnAl-T-NaOH cathode under a capacity limit of 500 mA h/g at 200 mA/g.

catalytic performance towards CO_2 hydrogenation, suggesting that the addition of thiourea during CuCoNiZnAl synthesis and alkali treatment after CuCoNiZnAl-T preparation is a reliable strategy for modifying HEOs to enhance CO_2 catalytic conversion.

As shown in Fig. 4(b), these HEO catalysts exhibit catalytic performances for CO oxidation that are similar to those for CO_2 hydrogenation. Firstly, all of them show increased CO conversion with increasing reaction temperature from 120 to 300 °C. In addition, CuCoNiZnAl-T-NaOH exhibits a higher CO conversion than CuCoNiZnAl and CuCoNiZnAl-T in the whole temperature range (especially between 160 and 220 °C). Over CuCoNiZnAl, CO conversion is only 2.2% and 28.5% at 160 and 200 °C, respectively, much lower than those of CuCoNiZnAl-T (6.3% and 55.6%, respectively) and CuCoNiZnAl-T-NaOH (18.1% and 91.2%, respectively). Furthermore, the CuCoNiZnAl-T-NaOH catalyst shows a much lower T50 and T90 (i.e., the temperatures for 50% and 90% CO conversion, respectively) than those of CuCoNiZnAl. Under same reaction condition, the T50 of CuCoNiZnAl-T-NaOH is 176 °C, which is lower than that of CuCoNiZnAl-T by 21 °C and that of CuCoNiZnAl by 36 °C. Apparently, CuCoNiZnAl-T-NaOH offers the best catalytic performance for CO oxidation, suggesting that the addition of thiourea in the HEOs along with alkali liquor treatment can optimize CO oxidation. Combined with the CO_2 hydrogenation results, it is reasonably deduced that the modulation of the HEOs produces a positive effect on the enhancement of the thermocatalytic redox reactions. More excitingly, CuCoNiZnAl-T-NaOH even delivers a much higher performance than that of CuCoNiZnAl-T in the glucose electrocatalysis oxidation reaction (Fig. S18), thereby demonstrating its applicability for a variety of catalytic reactions.

In addition, the Li-O_2 battery performances of these HEOs were examined through galvanostatic discharge and charge tests. Fig. 4(c) exhibits the initial full discharge/charge profiles of an Li-O_2 battery using CuCoNiZnAl, CuCoNiZnAl-T, and CuCoNiZnAl-T-NaOH as cathodes at 200 mA/g from 2.0 to 4.5 V *vs.* Li+/Li. Clearly, the Li-O_2 battery based on CuCoNiZnAl-T-NaOH has a lower overpotential (1.68 V) than those based on CuCoNiZnAl (1.77 V) and CuCoNiZnAl-T (1.73 V). Remarkably, the CuCoNiZnAl-T-NaOH cathode delivers much higher discharge/charge capacities of 12049/9901 mAh/g than those of CuCoNiZnAl-T (11917/8071 mAh/g) and CuCoNiZnAl (7260/5224 mAh/g), which is also better than most reported metal oxide electrode materials for Li-O_2 batteries (Table S1). Moreover, the CuCoNiZnAl-T-NaOH cathode gives the selected discharge/charge profiles under special conditions (Fig. 4(d)). Notably, the specific capacity remains nearly stable in a span of 100 cycles, much longer than that of CuCoNiZnAl-T (Fig. S19). By comparing the performances of the Li-O_2 batteries based on CuCoNiZnAl-T-NaOH and CuCoNiZnAl-T, it is evident that the former cathode demonstrates a more favorable cycling performance. In detail, the discharge/charge terminal voltage of the CuCoNiZnAl-T-NaOH cathode remains stable for as long as 2500 h (≈ 250 cycles) (Fig. 4(e)), much longer than that of the CuCoNiZnAl-T cathode (1600 h, ≈ 160 cycles) (Fig. S20) and most reported electrode materials (Table S1) [36–39]. Therefore, it is confirmed that CuCoNiZnAl-T-NaOH also holds huge potential as a promising electrode material for advanced Li-O_2 batteries.

3.4. Reaction mechanism

Based on the above, it is evident that the introduction of thiourea during the CuCoNiZnAl preparation process and the post alkali liquor treatment can activate some transition metal sites and O_{latt} species in the HEOs, further enhancing their performance in catalytic redox reactions and Li-O_2 batteries. To analyze the role of the activated transition metal sites and O_{latt} species in these HEOs with respect to catalytic performance, we characterized CuCoNiZnAl and CuCoNiZnAl-T using near ambient-pressure (NAP) XPS during the H_2 reduction, CO_2 adsorption, and hydrogenation. Although the CO_2 and H_2 pressures used in the characterizations are much lower than that of the actual reaction condition, they are sufficient to simulate the reactions over the HEO catalyst surface. Changes in the chemical states of the HEOs and the reaction intermediates were analyzed using NAP-XPS (Figs. S21–S24 and Fig. 5). After H_2 pre-treatment and CO_2 adsorption, it is clearly observed that CuCoNiZnAl-T enhances the C 1*s* band intensity at 293.0 eV, corresponding to gaseous CO_2 species (Fig. S21(b)) [40], which is in good agreement with the CO_2-TPD result (Fig. S25), indicating that CuCoNiZnAl-T has a stronger CO_2 adsorption ability than CuCoNiZnAl. Fig. S22 summarizes the observations of Cu 2*p* and auger electron spectroscopy in the NAP-XPS experiments. Both the CuCoNiZnAl and CuCoNiZnAl-T catalysts exhibit the core-level features at binding energies of 934 and 954 eV, corresponding to Cu^{2+} in the HEOs [41]. In addition, they all show a slight downshift to Cu^0 after H_2 pre-treatment and slight upshift to Cu^+ after CO_2 adsorption. Meanwhile, upon CO_2+H_2 treatment, the Cu 2*p* peak shifts slightly over both the CuCoNiZnAl and CuCoNiZnAl-T catalysts, indicating that the Cu species provide less electron transportation for CO_2 hydrogenation. A similar phenomenon was also observed in the Cu LMM auger electron spectra under the same condition. Meanwhile, the poor electron transport ability over the CuCoNiZnAl and CuCoNiZnAl-T catalysts for CO_2 hydrogenation was also observed in the Zn 2*p* and Al 2*p* XPS spectra (Figs. S23 and S24). Therefore, it is deduced that the Zn and Al species mainly play the role of structure promoter in the CuCoNiZnAl HEO for CO_2 hydrogenation.

As for the Co 2*p* and Ni 2*p* XPS signals, some additional interesting information was obtained during H_2 treatment, CO_2 adsorption, and reaction with CO_2 + H_2 over the CuCoNiZnAl and CuCoNiZnAl-T catalysts. As shown in Fig. 5(a), the peak centered at 779.6 eV was ascribed to Co $2p_{3/2}$ of Co_3O_4. The peak at 779.6 eV was split into two peaks at 780.5 and 778.2 eV, assigned to Co^{2+} and Co^0, respectively [42,43]. It is suggested that the Co oxides were reduced, and CoO as well as Co coexisted on the matrix surface under H_2 pre-treatment at 400 °C. Afterwards, Co was oxidized to CoO when introducing CO_2. However, there is only slight upshift of binding energy (0.1 eV) of Co $2p_{3/2}$ over the CuCoNiZnAl catalyst from CO_2 adsorption to the CO_2 + H_2 reaction. As for the Ni 2*p* spectra acquired for

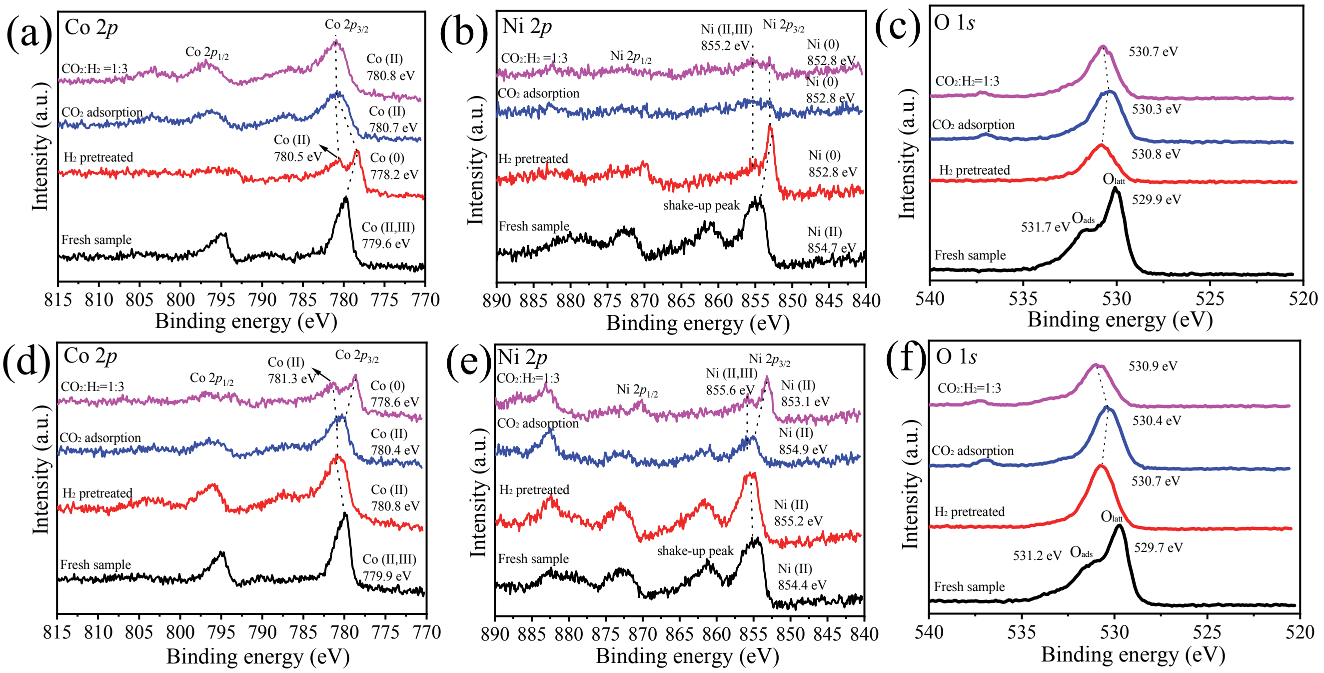

Fig. 5. *In-situ* Co 2*p* (a), Ni 2*p* (b), and O 1*s* (c) XPS spectra of CuCoNiZnAl, and Co 2*p* (d), Ni 2*p* (e), and O 1*s* (f) XPS spectra of CuCoNiZnAl-T in contact with 0.1 mbar H_2 at 400 °C, 0.1 mbar CO_2 at 350 °C, and 0.4 mbar of CO_2 (0.1 mbar) + H_2 (0.3 mbar) at 350 °C.

the reactions over the CuCoNiZnAl catalyst, Ni oxides were also reduced under H_2 pretreatment, and the resultant Ni species were further oxidized when introducing CO_2. However, the formed Ni oxides may possibly be coated by the other metal species and almost do not participate in the CO_2 hydrogenation reaction (Fig. 5(b)). In addition, it is obvious that the oxygen species could be reduced or oxidized by introducing H_2/CO_2+H_2 or CO_2, respectively (Fig. 5(c)). In detail, the O_{ads} sites are possibly reduced by introduced H_2, which indirectly indicates that only O_{latt} participate in the CO_2 hydrogenation reaction. In rapid sequence, the O 1*s* binding energy changes from 530.8 to 530.3 eV when introducing CO_2 and shifts from 530.3 to 530.7 eV in the presence of CO_2 + H_2.

Compared with the evolution of the Co 2*p*, Ni 2*p*, and O 1*s* XPS spectra over the CuCoNiZnAl catalyst during the simulation of the CO_2 hydrogenation process, the CuCoNiZnAl-T catalyst undergoes some different phenomena under the same condition. At first, the existing Co and Ni oxides of the CuCoNiZnAl-T catalyst are the same as that of CuCoNiZnAl (Figs. 5(d) and (e)). However, the Co_3O_4 of the CuCoNiZnAl-T catalyst could be only reduced to CoO after H_2 treatment, and the generated CoO species almost does not react with the introduced CO_2. Meanwhile, upon injecting H_2, not only does the binding energy of Co 2$p_{3/2}$ of CoO shifts upwards from 780.4 to 781.3 eV, but Co is also formed. This indicates that the enhanced electron transfer, derived from the changed Co species, performs well over the CuCoNiZnAl-T catalyst during the CO_2 hydrogenation process. Similarly, active electron transferability was also observed on the Ni oxides over CuCoNiZnAl-T during the CO_2 hydrogenation process. Compared with CuCoNiZnAl, the CuCoNiZnAl-T catalyst still clearly exhibits Ni oxide peaks in the XPS spectra after introducing CO_2. Also, the peak at 854.9 eV is divided into two peaks at 855.6 and 853.1 eV upon injecting CO_2+H_2, suggesting that abundant electrons through the change in Ni oxides participate in CO_2 hydrogenation [43–45]. Affected by the activated Co and Ni species, the O 1*s* XPS peak of the CuCoNiZnAl-T catalyst undergoes a binding energy shift of 0.5 eV upon the change from CO_2 to CO_2 + H_2 (0.4 eV for CuCoNiZnAl). It is concluded that the O_{latt} species of the CuCoNiZnAl-T catalyst is more active than that of the CuCoNiZnAl catalyst. Based on the above, it is believed that the activated Co and Ni species along with enhanced O_{latt} species could efficiently establish a more fluent channel of electron transfer over the CuCoNiZnAl-T catalyst than that of CuCoNiZnAl, thus promoting CO_2 hydrogenation.

Aside from the physical-chemical properties and catalytic redox and energy storage performance of the HEO catalysts, we further investigated the underlying reasons for the enhanced performance and briefly propose the possible mechanism of CO_2 hydrogenation reaction over the CuCoNiZnAl-T catalyst (Fig. 6). According to the H_2-TPR and Raman results (Figs. 1(c) and (d)), it is confirmed that the introduction of thiourea during the preparation process optimizes the reduction ability of the Co and Ni oxides. Furthermore, the NAP-XPS results also prove that the activated Co/Ni oxides and O_{latt} species play key roles in CO_2 hydrogenation over the CuCoNiZnAl-T catalyst. From the CO_2-TPD and H_2-TPD results (Figs. S25 and S26), we also observed that CuCoNiZnAl-T possesses a stronger adsorp-

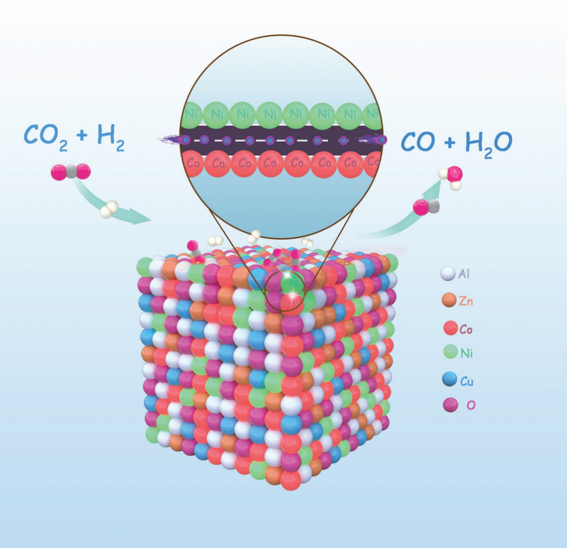

Fig. 6. Mechanism of CO_2 hydrogenation over CuCoNiZnAl-T catalyst.

tion ability and more adsorption sites under CO_2 and H_2 than that of the CuCoNiZnAl catalyst, particularly for CO_2. During the CO_2 hydrogenation reaction, the increased number of basic sites of the CuCoNiZnAl-T catalyst bind with CO_2 to generate adsorbed species (Fig. S21(b)). Meanwhile, the adsorbed CO_2 species reacted with H_2 at the activated O_{latt} species from the activated Co and Ni oxides. Subsequently, the constant changing of different Co oxides and Ni oxides under CO_2 and H_2 built a passageway for electron transport, consequently promoting the CO_2 hydrogenation process (Fig. 6). Therefore, the CuCoNiZnAl-T catalyst exhibits much better catalytic activity for CO_2 hydrogenation than CuCoNiZnAl (Fig. 4(a) and Fig. S15). Meanwhile, it was revealed that the crystal structure of the CuCoNiZnAl-T used catalyst is slightly different from that of CuCoNiZnAl-T (Fig. S27). In detail, the diffraction peaks of the MO_x phase disappeared, suggesting that it is possibly reduced by H_2 under the reaction process. Combined with the HRTEM and XRD results, it is deduced that only the spinel phase in the HEOs plays a key role in the CO_2 hydrogenation catalytic reaction. As for CuCoNiZnAl-T-NaOH, not only the Co and Ni oxides but also the Cu oxides were released and activated by constructing a sheet-like morphology (Figs. 1(c) and (d)). Owing to the coexistence of activated Cu oxides, Co oxides, and Ni oxides, as well as O_{latt} species, the CuCoNiZnAl-T-NaOH catalyst shows the best catalytic performance for both CO_2 hydrogenation and CO oxidation among the three HEOs. In contrast with the CO_2 hydrogenation activity results (CuCoNiZnAl-T-NaOH ≈ CuCoNiZnAl-T > CuCoNiZnAl), the CO oxidation performance over these HEOs catalysts decreases in the order CuCoNiZnAl-T-NaOH > CuCoNiZnAl-T > CuCoNiZnAl, which could be explained by the fact that the Cu species is the most active for CO oxidation, while the Co and Ni species are more active for CO_2 hydrogenation [43,46–48]. Moreover, the abundant activated O_{latt} species of CuCoNiZnAl-T-NaOH also contribute well to the CO catalytic oxidation conversion [49]. Meanwhile, the superior electron transport ability derived from the activated Cu, Co, Ni oxides and O_{latt} species also endows CuCoNiZnAl-T-NaOH with the highest discharge/charge capacity (12049/9901 mAh/g) and excellent stability (2500 h) as a cathode material for an Li-O_2 battery.

4. Conclusions

In summary, we developed a general effective and environmentally friendly strategy to directly modulate the chemical states of the Co and Ni sites in CuCoNiZnAl HEOs simply by adding thiourea in a solvent-free process. Meanwhile, the post alkaline solution treatment further activated Cu species by constructing a sheet-like structure of the CuCoNiZnAl-T HEOs. Subsequently, we utilized H_2-TPR, electron microscopy, and XPS techniques to directly determine the change in morphological features and physical-chemical properties of the CuCoNiZnAl-T and CuCoNiZnAl-T-NaOH HEOs, further establishing the relationship between the optimized physical-chemical properties and catalytic redox performance. As a result, the introduced thiourea and alkaline solution treatment contribute well to the activation of Cu, Co, and Ni oxides along with O_{latt} species. By virtue of these optimized characteristics, the CuCoNiZnAl-T-NaOH HEOs catalyst shows superior catalytic performance for CO_2 hydrogenation, CO oxidation, and use as a cathode in a Li-O_2 battery compared with CuCoNiZnAl and CuCoNiZnAl-T. Clearly, its excellent performance is mainly attributed to the more facile electron transfer between Cu/Ni/Co sites and O_{latt} species in its framework, significantly promoting its redox properties. In conclusion, this work optimized HEOs with targeted activated metal sites as highly active heterogeneous thermal and electrochemical catalysts for redox reactions and energy storage.

Acknowledgments

The authors thank Prof. Yi Cui and Zhongmiao Gong in the Vacuum Interconnected Nanotech Workstation (NANO-X) (Suzhou Institute of Nanotechnology and Nano-bionics, Chinese Academy of Sciences) for kindly conducting NAP-XPS characterization.

Electronic supporting information

Supporting information is available in the online version of this article.

References

[1] Y. F. Sun, S. Dai, *Sci. Adv.*, **2021**, 7, eabg1600.
[2] S. H. Albedwawi, A. AlJaberi, G. N. Haidemenopoulos, K. Polychronopoulou, *Mater. Des.*, **2021**, 202, 109534.
[3] M. S. Fu, X. Ma, K. N. Zhao, X. Li, D. Su, *iScience.*, **2021**, 24, 102177.
[4] Y. Wang, J. X. Mi, Z.-S. Wu, *Chem Catal.*, **2022**, 2, 1624–1656.
[5] C. M. Rost, E. Sachet, T. Borman, A. Moballegh, E. C. Dickey, D. Hou, J. L. Jones, S. Curtarolo, J.-P. Maria, *Nat. Commun.,* **2015**, 6, 8485.
[6] A. Sarkar, Q. S. Wang, A. Schiele, M. R. Chellali, S. S. Bhattacharya, D. Wang, T. Brezesinski, H. Hahn, L. Velasco, B. Breitung, *Adv. Mater.*, **2019**, 31, 1806236.
[7] Y. Shu, J. F. Bao, S. Z. Yang, X. L. Duan, P. F. Zhang, *AIChE J.*, **2020**,

Graphical Abstract

Chin. J. Catal., 2023, 48: 235–246 doi: 10.1016/S1872-2067(23)64409-2

Activation of partial metal sites in high-entropy oxides for enhancing thermal and electrochemical catalysis

Jinxing Mi, Xiaoping Chen, Yajun Ding, Liangzhu Zhang, Jun Ma, Hui Kang, Xianhong Wu, Yuefeng Liu, Jianjun Chen * , Zhong-Shuai Wu *
Dalian Institute of Chemical Physics, Chinese Academy of Sciences; Tsinghua University

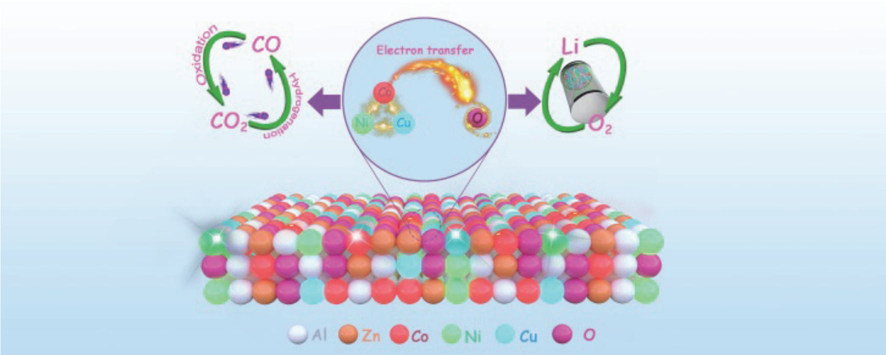

The lamellar CuCoNiZnAl-T-NaOH high entropy oxide with activated Cu, Co, and Ni oxides species accompanied with enriched lattice oxygen species displays remarkably improved performance of redox catalysis and Li-O$_2$ battery.

67, e17046.

[8] K. Z. Gu, D. D. Wang, C. Xie, T. H. Wang, G. Huang, Y. B. Liu, Y. Q. Zou, L. Tao, S. Y. Wang, *Angew. Chem. Int. Ed.,* **2021**, 60, 20253–20258.

[9] E. Lokcu, C. Toparli, M. Anik, *ACS Appl. Mater. Interfaces,* **2020**, 12, 23860–23866.

[10] H. Chen, K. C. Jie, C. J. Jafta, Z. Z. Yang, S. Y. Yao, M. M. Liu, Z. H. Zhang, J. X. Liu, M. F. Chi, J. Fu, S. Dai, *Appl. Catal. B*, **2020**, 276, 119155.

[11] Y. J. Ma, Y. Ma, S. L. Dreyer, Q. S. Wang, K. Wang, D. M. Goonetilleke, A. Omar, D. Mikhailova, H. Hahn, B. Breitung, T. Brezesinski. *Adv. Mater.*, **2021**, 33, 2101342.

[12] H. D. Xu, Z. H. Zhang, J. X. Liu, C.-L. Do-Thanh, H. Chen, S. H. Xu, Q. J. Lin, Y. Jiao, J. L. Wang, Y. Wang, Y. Q. Chen, S. Dai, *Nat. Commun.*, **2020**, 11, 3908.

[13] Z. Zhang, S. Yang, X. Hu, H. Xu, H. Peng, M. Liu, B. P. Thapaliya, K. Jie, J. Zhao, J. Liu, H. Chen, Y. Leng, X. Lu, J. Fu, P. F. Zhang, S. Dai, *Chem. Mater.*, **2019**, 31, 5529–5536.

[14] T. Wang, H. Chen, Z. Yang, J. Liang, S. Dai, *J. Am. Chem. Soc.,* **2020**, 142, 4550–4554.

[15] H. Chen, J. Fu, P. Zhang, H. Peng, C. W. Abney, K. Jie, X. Liu, M. Chi, S. Dai, *J. Mater. Chem. A.,* **2018**, 6, 11129–11133.

[16] F. Okejiri, Z. Zhang, J. Liu, M. Liu, S. Yang, S. Dai, *ChemSusChem*, **2020**, 13, 111–115.

[17] H. Chen, Y. Sun, S. Yang, H. Wang, W. Dmowski, T. Egami, S. Dai, *Chem. Commun.*, **2020**, 56, 15056–15059.

[18] F. Tavani, M. Fracchia, A. Tofoni, L. Braglia, A. Jouve, S. Morandi, M. Manzoli, P. Torelli, P. Ghigna, P. D'Angelo, *Phys. Chem. Chem. Phys.*, **2021**, 23, 26575–26584.

[19] S. Hou, X. Ma, Y. Shu, J. Bao, Q. Zhang, M. Chen, P. Zhang, S. Dai, *Nat. Commun.*, **2021**, 12, 5917.

[20] H. Chen, W. Lin, Z. Zhang, K. Jie, D. R. Mullins, X. Sang, S.-Z. Yang, C. J. Jafta, C. A. Bridges, X. Hu, R. R. Unocic, J. Fu, P. F. Zhang, S. Dai, *ACS Mater. Lett.*, **2019**, 1, 83–88.

[21] D. Lan, M. Qin, J. L. Liu, G. L. Wu, Y. Zhang, H. J. Wu, *Chem. Eng. J.*, **2020**, 382, 122797.

[22] J. H. Zhu, J. Jiang, Z. P. Sun, J. S. Luo, Z. X. Fan, X. T. Huang, H. Zhang, T. Yu, *Small*, **2014**, 10, 2937–2945.

[23] C. Jin, Y. X. Cui, G. F. Zhang, W. H. Luo, Y. X. Liu, Y. Sun, Z. M. Tian, W. J. Zheng, *Chem. Eng. J.*, **2018**, 343, 331–339.

[24] M. de Santana Santos, R. C. R. Neto, F. B. Noronha, P. Bargiela, M. G. C. da Rocha, C. Resini, E. Carbo-Argibay, R. Frety, S. T. Brandao, *Catal. Today*, **2018**, 299, 229–241.

[25] C. H. Mejia, J. E. S. van der Hoeven, P. E. de Jongh, K. P. de Jong, *ACS Catal.*, **2020**, 10, 7343–7354.

[26] W. Jeon, I.-H. Choi, J.-Y. Park, J.-S. Lee, K.-R. Hwang, *Catal. Today*, **2020**, 352, 95–103.

[27] M. Jablonska, M. Nocun, K. Golabek, R. Palkovits, *Appl. Surf. Sci.*, **2017**, 423, 498–508.

[28] A. V. Fedorov, R. G. Kukushkin, P. M. Yeletsky, O. A. Bulavchenko, Y. A. Chesalov, V. A. Yakovlev, *J. Alloys Compd.*, **2020**, 844, 156135.

[29] D. M. Meng, Q. Xu, Y. L. Jiao, Y. Guo, Y. L. Guo, L. Wang, G. Z. Lu, W. C. Zhan, *Appl. Catal. B*, **2018**, 221, 652–663.

[30] M.-K. Son, L. Steier, M. Schreier, M. T. Mayer, J. S. Luo, M, Gra¨tzel. *Energy Environ. Sci.*, **2017**, 10, 912–918.

[31] N. J. Usharani, A. Bhandarkar, S. Subramanian, S. S. Bhattacharya, *Acta Mater.*, **2020**, 200, 526–536.

[32] X. H. Zhang, C. L. Pei, X. Chang, S. Chen, R. Liu, Z.-J. Zhao, R. T. Mu, *J. Am. Chem. Soc.*, **2020**, 142, 11540–11549.

[33] X. Q. Liu, J. X. Mi, L. Shi, H. Y. Liu, J. Liu, Y. Ding, J. Q. Shi, M. H. He, Z. S. Wang, S. C. Xiong, Q. F. Zhang, Y. F. Liu, Z.-S. Wu, J. J. Chen, J. H. Li, *Angew. Chem. Int. Ed.*, **2021**, 60, 26747–26754.

[34] S. Royer, D. Duprez, F. Can, X. Courtois, C. Batiot-Dupeyrat, S. Laassiri, H. Alamdari, *Chem. Rev.*, **2014**, 114, 10292–10368.

[35] C. Dong, Z. Qu, Y. Qin, Q. Fu, X. Duan, *ACS Catal.*, **2019**, 9, 6698–6710.

[36] W. Zhao, X. M. Li, R. Yin, L. Qian, X. S. Huang, H. Liu, J. X. Zhang, J. Wang, T. Ding, Z. H. Guo. *Nanoscale*, **2019**, 11, 50–59.

[37] X. M. Liu, L. L. Zhao, H. R. Xu, Q. S. Huang, Y. Q. Wang, C. X. Hou, Y. Y. Hou, J. Wang, F. Dang, J. T. Zhang. *Adv. Energy Mater.*, **2020**, 10,

2001415.

[38] R. Gao, Q. Z. Chen, W. J. Zhang, D. Zhou, D. Ning, G. Schumacher, D. Smirnov, L. M. Sun, X. F. Liu. *J. Catal.*, **2020**, 384, 199–207.

[39] M. Balaish, J.-W. Jung, I.-D. Kim, Y. Ein-Eli, *Adv. Funct. Mater.*, **2020**, 30, 1808303.

[40] L. X. Wang, E. Guan, Y. Q. Wang, L. Wang, Z. M. Gong, Y. Cui, X. J. Meng, B. C. Gates, F. S. Xiao. *Nat. Commun.*, **2020**, 11, 1033.

[41] W. J. Zhang, M. H. Jiang, S. Y. Yang, Y. Hu, B. Mu, Z. X. Tie, Z. Jin, *Nano Res. Energy*, **2022**, 1, e9120033.

[42] S. Q. Zhao, J. J. Lin, P. Wu, C. C. Ye, Y. F. Li, A. Q. Li, X. J. Jin, Y. Zhao, G. X. Chen, Y. C. Qiu, D. Q. Ye, *ACS Appl. Mater. Interfaces*, **2021**, 13, 48764–48773.

[43] C. J. Powell, *J. Electron Spectrosc. Relat. Phenom.*, **2012**, 185, 1–3.

[44] S. A. Vladimirova, K. Y. Prikhodko, M. N. Rumyantseva, E. A. Konstantinova, A. S. Chizhov, N. O. Khmelevsky, A. M. Gaskov, *J. Alloys Compd.*, **2020**, 828, 154420.

[45] A. Sapi, G. Halasi, J. Kiss, D. G. Dobo, K.L. Juhasz, V. J. Kolcsar, Z. Ferencz, G. Vari, V. Matolin, A. Erdohelyi, A. Kukovecz, Z. Konya, *J. Phys. Chem. C*, **2018**, 122, 5553–5565.

[46] S. Kattel, P. J. Ramirez, J. G. G. Chen, J. A. Rodriguez, P. Liu, *Science*, **2017**, 355, 1296–1299.

[47] L. R. Winter, E. Gomez, B. H. Yan, S. Y. Yao, J. G. G. Chen, *Appl. Catal. B*, **2018**, 224, 442–450.

[48] R.-P. Ye, J. Ding, W. B. Gong, M. D. Argyle, Q. Zhong, Y. J. Wang, C. K. Russell, Z. H. Xu, A. G. Russell, Q. H. Li, M. H. Fan, Y. G. Yao. *Nat. Commun.*, **2019**, 10, 5698.

[49] Q. Liu, J. X. Mi, X. P. Chen, S. H. Wang, J. J. Chen, J. H. Li, *Chem. Eng. J.*, **2021**, 423, 130228.

活化高熵氧化物中部分金属位点显著增强热催化和电催化

米金星[a,1], 陈孝平[b,1], 丁亚军[a], 张良柱[a], 马军[c], 康辉[c], 吴粕虹[a], 刘岳峰[c],
陈建军[b,*], 吴忠帅[a,*]

[a]中国科学院大连化学物理研究所, 催化基础国家重点实验室, 辽宁大连116023
[b]清华大学环境学院, 环境模拟与污染控制国家重点联合实验室, 北京100084
[c]中国科学院大连化学物理研究所, 洁净能源国家实验室(筹), 辽宁大连116023

摘要: 高熵氧化物(HEOs)作为一种新兴材料受到科研工作者的广泛关注, 并推动了高熵陶瓷材料(碳化物、硫化物、氟化物等)的发展及其在介电、磁学、储氢以及能源转化等领域中的应用. 其中, HEOs由于丰富的活性位点、可调节的比表面积、稳定的晶体结构、独特的几何相容性和电子结构等特性在催化化学领域展示出广阔的应用前景. 然而, 受制于HEOs的结构特点和难以精确调控的物化性质, 当前的研究主要围绕HEOs制备方法的探索及其在不同催化反应中的尝试. 在以HEOs为基体进行的催化反应中, 也有将贵金属与HEOs复合进行催化剂制备和催化应用的研究报道, 但效果并不理想. 因此, 如何直接对HEOs进行改性并提升其催化性能是低成本高效促进HEOs在催化领域发展的重要途径.

本文首先采用固相燃烧法制备CuCoNiZnAl HEOs, 同时在制备过程中加入硫脲后通过焙烧处理来进行物化性质的原位调节(记为CuCoNiZnAl-T), 随后采用碱液对CuCoNiZnAl-T处理来实现形貌的改变和物化性质的进一步优化(记为CuCoNiZnAl-T-NaOH). X射线粉末衍射结果表明, 硫脲添加和碱处理未改变CuCoNiZnAl-T-NaOH的晶型结构. 电镜结果表明, CuCoNiZnAl和CuCoNiZnAl-T均呈现出较大的颗粒状, 而CuCoNiZnAl-T-NaOH具有大片层形貌结构和明显的晶格扭曲. 此外, H_2程序升温还原、X射线光电子能谱和He程序升温脱附结果表明, CuCoNiZnAl-T-NaOH不仅具有容易还原的铜、镍、钴的氧化物物种, 而且具有高含量和更活泼的晶格氧物种. 因此, CuCoNiZnAl-T-NaOH在活性测试中展示出较好的CO_2加氢和CO氧化催化性能. 其中CuCoNiZnAl-T-NaOH在催化CO氧化反应中, 当转化率达到50%时所需转化温度为176 °C, 比相同条件下CuCoNiZnAl和CuCoNiZnAl-T作为催化剂达到同样催化效果时所需转化温度分别低36和21 °C. 此外, 当CuCoNiZnAl-T-NaOH用作锂氧电池电极材料时也展示出较好的电催化活性(放电/充电容量为12049/9901 mAh/g)和循环稳定性(2500 h). 随后, 以CO_2加氢反应为研究对象, 进一步采用近常压X射线光电子能谱进行反应机理分析, 结果表明, 相对于CuCoNiZnAl而言, CuCoNiZnAl-T在CO_2加氢反应过程中表面镍和钴的氧化物物种与活化的晶格氧之间更容易进行电子转移, 这种增强的电子传输能力和更强的CO_2吸附能力有利于CO_2加氢反应的进行. 推断这种电子传输能力的提升同样有利于CO氧化和锂氧电池性能的提升. 综上, 本文为HEOs催化剂的简洁制备和物化性质改善提供了技术借鉴, 有望进一步推进HEOs的改性制备和在其他领域的功能化应用发展.

关键词: 高熵氧化物; 固相燃烧法; 金属位点活化; 催化氧化还原; 锂氧电池

收稿日期: 2022-01-03. 接受日期: 2022-02-08. 上网时间: 2023-04-20.

*通讯联系人. 电子信箱: wuzs@dicp.ac.cn (吴忠帅), chenjianjun@tsinghua.edu.cn (陈建军).

[1]共同第一作者.

基金来源: 中国博士后科学基金(2021M693125); 大连市高层次人才创新支持计划(2019RT09); 中国科学院洁净能源创新研究院合作基金(DNL202016, DNL202019); 中国科学院洁净能源创新研究院-榆林学院联合基金(YLU-DNL Fund 2021002, YLU-DNL Fund 2021009).